Final manuscript for Physics of Fluids, Vol. 6, no. 1, January 1994, 263-276

Experiments on the instabilities of a swirling jet

By J. Panda[1] and D. K. McLaughlin

The Pennsylvania State University, PA 16802, USA

Abstract

Instabilities present in a free-swirling jet in the Reynolds number range from 20,000 to 60,000 and a nominal swirl number of 0.5 are studied experimentally, using smoke visualization and hot-wire anemometry. Flow visualization photographs show vortex breakdown at the core and rolling up of the shear layer around the jet into weak, irregular, large scale organized structures. When forced by acoustic excitation these structures become energetic and periodic. Axisymmetric and helical instability waves in the Strouhal number range 0.75 to 1.5 are excited and their evolution along the axial direction are measured from velocity spectra and ensemble averaged measurements. Compared to a nonswirling jet, the overall growth of the instability waves are considerably smaller, and vortex pairing is suppressed in a swirling jet. However, the overall spread and mass entrainment rates are higher in the latter.

Measurements of the mean velocity components and turbulence fluctuations show that the vortex breakdown affects the axial velocity distribution and rapidly replaces the potential core with a large amount of turbulence. Upon interacting with the vortex breakdown, the shear layer along the jet periphery loses its organized structure and, in general, "random turbulence" follows.

INDEX: 47.20.Cq; 47.20.Ft; 47.27.Wg

1. Introduction

During the past three decades, there have been numerous studies of the instabilities and the organized turbulent structures in free shear flows such as two-dimensional mixing layers, round, elliptic and rectangular free jets. Despite the large number of studies of the free nonswirling jets, there is a lack of information on organized structures in swirling jets. The flow field of the latter is much more complex. In addition to the velocity gradients, the shear layer is subjected to curvature effects from the azimuthal component of velocity. The latter also imposes a radial pressure gradient, which is expected to modify the shear layer development of the free swirling jet. For a high swirl number jet where the azimuthal velocity component is comparable to the axial component of velocity, vortex bursting may appear in the jet core (Chervinsky and Chigier 1966). It is

[1] Current address: NASA Lewis Research Center, Cleveland, OH 44135, USA.

found that vortex bursting is an additional phenomenon that makes the development of a swirling jet unique among all shear flows. The present experimental investigation represents an initial effort to develop an understanding of the instability waves and organized turbulent structures present in a round, free-swirling jet.

Swirl is imparted to flows in many practical devices including combustors and cyclone separators. It is an undesirable feature of aircraft wake flows and is observed frequently in natural flows such as in tornadoes. Swirling jets may also find application in the jet engine exhaust plume, where a faster spreading and quicker mixing is desirable. The rich varieties of flow features including turbulent structures, observed in swirling flows, are not well understood. An improvement of our understanding of the complex, turbulent flow field should facilitate the designs of various practical devices.

In the past, the major focus of most experimental (Rose 1962; Chervinsky and Chigier 1966; Sislian and Cusworth 1986) and computational (e. g. Rhode 1981) studies was to measure or calculate the time mean flow fields and various turbulent stresses. Such studies revealed some interesting behavior characteristic of swirling jets, such as a strong reverse flow at the center of the jet starting at the nozzle exit (Sislian and Cusworth 1986), a gradual change of the axial velocity profile with an increase of the swirl velocity (Chervinsky and Chigier 1966) and a high spreading rate of such jets (Rose 1962). Vortex bursting produces reverse flow, but the cause of the latter two effects is not very clear. A limited amount of experimental work on the instability waves in the shear layer around a low swirl number (S = 0.12) free-swirling jet of Re = 4.6×10^5 was reported by Taghavi and Rice (1989). The primary purpose of their experiment was to increase the spreading rate by plane wave acoustic excitation. They found that a very high level of excitation is needed to affect the spreading rate of a free-swirling jet. They also noted that the subharmonic of the excitation frequency showed very little growth in such jets. The experiments were limited in scope and the detailed characteristics of the organized structures were not studied.

The present authors know of no hydrodynamic stability analysis of the shear layer around a free-swirling jet that is reported in the literature. Lessen *et al.* (1974), Leibovich and Stewartson (1983), and Khorrami (1991) have studied the hydrodynamic stability of a trailing line vortex. The axial and azimuthal velocity distributions in such a vortex are different from those of the free-swirling jet under consideration. Two important results, common to all of the aforementioned stability calculations are large amplification rates of helical instability waves of negative wave numbers (i.e. waves whose phase fronts move opposite to the mean flow rotation) and suppression of all other modes even at a small swirl number. Good experimental data to substantiate such results, however, is unavailable at this time.

The objectives of the present study are twofold. The first and the primary objective is to develop an understanding of the Kelvin-Helmholtz instability waves and the organized structures present in the near field

of a free-swirling jet. For this purpose, low Reynolds number (Re = 20,000 to 60,000) and relatively high swirl number (S ~ 0.5) swirling jets are studied. A further increase of swirl number produces a highly turbulent jet, in the Reynolds number range of study, due to vortex bursting inside the tunnel. Therefore, maximum swirl number is kept limited to 0.5. The organized structures of various mode shapes are visualized and their evolution is measured using hot-wire anemometry under the influence of artificial acoustic excitation. The methodologies used to explore these structures are similar to those used by Browand and Laufer (1975), Kibens (1979), Hussain and Zaman (1985) among others. It is observed that swirl makes the organized structures weaker and suppresses vortex pairing.

The second objective is to determine the effect of vortex bursting on the jet characteristics and the coherent structures. Vortex bursting is primarily studied through flow visualization and its effects on the time mean velocity distributions and turbulence fluctuations are also measured.

Somewhat detailed experiments were also conducted on nonswirling jets of Re = 29,000 and 60,000 to validate the experimental procedures and also to obtain data for direct comparison. Except for a limited comparison, these data are not presented here and can be found in the thesis of Panda (1990).

In this study, attention is focused on the near jet region $0 \leq x/D \leq 2.5$. Hence, the jet column instability mode of the swirling jet is not explored.

2. Experimental facility, procedures and operating conditions

The present experiments are conducted in a vertically oriented wind tunnel as shown schematically in figure 1. There is an axial flow fan at the bottom of the tunnel that drives the air flow. The air passes through a flow conditioning section, a diffuser, a turbulence management section, swirl vanes and finally through a contraction section to the 15.2 centimeter (6") diameter exit. The swirler consists of 20 turning vanes each mounted independently on the centerbody and fixed at one turning angle throughout the experiment. The vanes along with the centerbody are removed to produce nonswirling jets from the same facility. The centerbody is hollow with tubes inserted into it to inject smoke from an outside source. The centerbody terminates 27 cm upstream of the nozzle exit.

In order to avoid strong wake from the centerbody and the turning vanes, they were placed inside the contraction far upstream of the nozzle exit. Moreover, the jet Reynolds number, based on the nozzle diameter is sufficiently low (Re ≤ 60,000) for the shear layer at the nozzle exit to be laminar; yet it has a relatively high turbulence intensity. The peak axial velocity fluctuations at the nozzle exit are 15% and 18% of the mass averaged axial velocity for respectively, Re = 22,000 and 57,000 jets. This high turbulence level, however, sharply decreases away from the shear layer inside the potential flow region of the jet. (Measurements of the

turbulent fluctuations are presented later in figure 10). By inserting a hot-wire probe at various locations inside the tunnel, it was observed that local flow separation occurred on the wall of the contraction section downstream of the swirl producing vanes. Possibly, the tip vortices from the vanes and the extra azimuthal curvature of the streamlines affect the performance of the contraction section leading to the local flow separation. It is suspected that the flow separation occurs on the swirl vanes, which are set at a high turning angle. The combined effect of the various disturbances, upstream flow separation and low Reynolds number operation is to produce a disturbed shear layer with relatively high turbulence fluctuations at the nozzle exit. Details of the tunnel construction flow unsteadiness and contraction separation are discussed in the thesis of Panda (1990).

The fundamental Helmholtz resonance frequency of the tunnel is calculated to be approximately 24 Hz. Spectra of microphone signals located inside the contraction section show three humps around 20, 108 and 173 Hz, which correspond to the tunnel resonance frequencies. For the most part they are separated from the Kelvin-Helmholtz instability frequencies of interest.

The artificial excitation system: The excitation system consists of four large acoustic speakers arranged circumferentially around the jet exit as shown in figure 1. The perturbations are introduced 11 cm from the centerline (3.5 cm from the nozzle lip line) through a 6 mm slot. To perturb the shear layer with disturbances of different azimuthal mode shapes, the speakers are operated with various phase combinations. This is achieved by using a phase shifting circuit as described in Panda (1990). This technique was proven successful by Bechert and Pfizenmaier (1976), among others.

The level of acoustic excitation is determined from the non-dimensionalized fluctuating acoustic velocity introduced at the jet centerline by the external excitation. The fluctuating acoustic velocity A, is approximately evaluated as acoustic pressure p_{ac} divided by the characteristic impedance (density ρ_o times the speed of sound a_o) of air. Thus,

$$A = \frac{\text{Fluctuating acoustic velocity}}{\text{Mean jet velocity}} \times 100\%$$

$$\approx \frac{p_{ac}}{(\rho_o a_o) \times \overline{U}} \times 100\%$$

The sound pressure levels are measured with a 0.5 inch microphone placed at the center of the nozzle exit perpendicular to the plane containing the speakers. For measurements with in-phase excitation the phase of the acoustic waves emanating from the speaker boxes are within ± 5° of one another. The difference in the sound pressure level produced by individual speakers is less than ± 1 dB.

Swirl number, Reynolds number and the operating conditions: Usually, a non-dimensional swirl number S (Gupta and Lilley 1985), defined below, is used to represent the relative amount of swirl present in a flow.

$$S = \frac{\text{Axial flux of tangential momentum } (\dot{G}_\theta)}{(\text{Radius}) \cdot (\text{Axial flux of axial momentum } (\dot{G}_x))}$$

$$\dot{G}_x = 2\pi \int_0^\infty (\rho U^2 + P) r\, dr$$

$$\dot{G}_\theta = 2\pi \int_0^\infty \rho U W r^2\, dr$$

Since S represents a ratio of two integrated quantities, two free-swirling jets of completely different velocity distributions may have the same swirl number (Farokhi *et al.* 1989). Thus the use of swirl number to generalize the behavior of all swirling jets is somewhat imperfect. Nevertheless, S, as defined above, is commonly used in the literature of swirling flows and is also used here. The Reynolds number Re = UD/v is defined based on the mass averaged axial velocity U and the nozzle diameter D.

Table 1 shows the operating conditions for which excitation is applied to the jet. Low levels of excitation are used for the quantitative measurements, while higher levels of excitation are used for the flow visualizations. All measurements are done at the tabulated Reynolds numbers, however, flow visualization at few other Reynolds number are also presented.

Flow visualization and hot-wire measurements: Flow visualization is performed by two different methods. In the smoke wire technique (Cimbala 1984 and Corke *et al.* 1977), a 0.13 mm diameter stainless steel wire is placed horizontally either across the diameter of the nozzle exit (`straight wire', figure 2a) or around the nozzle lip just inside the flow (`circular wire', figure 2b). For the latter, the wire is supported by 16 leads with small loops at the supporting ends. The steel wire is passed through these loops to make it nearly circular, although it is effectively a sixteen-sided polygon. The smoke streaks are illuminated by flashes from a Strobe light. For the multiple exposure photographs of the excited jet, the Strobe is externally triggered at the excitation frequency while the camera shutter is kept open for a long time.

The smoke injection method is primarily used to visualize vortex bursting at the jet core. In this technique, a cigarette is lit in a compressed air flow inside a flask and the generated smoke is carried to the hollow centerbody through one of the hollow supporting struts. The trailing edge of the centerbody has a small hole through which smoke can be injected into the flow. This smoke travels downstream along the centerline without any significant diffusion into other parts of the jet. The photographic technique is the same as that used with the smoke wire technique.

All quantitative measurements are performed using hot-wire probes with DISA 55M01 constant temperature anemometers. Probe calibration and the data reduction for 2-sensor probes are performed following the method of Westphal and Mehta (1984).

3. Results and discussions

3.1. Flow visualization of natural jets

Although many photographs are taken over a wide range of Reynolds number for both the nonswirling and the swirling jets, only those which best illustrate the physics are presented here. Flow is either from left to right or from bottom to top in the photographs.

Non-swirling jet: Figure 3 shows single exposure photographs of natural nonswirling jets at Re = 29,000. The duration time for a single flash is 10 microseconds, which effectively freezes the low speed flow. The `straight wire' photograph of figure 3a shows a cross-sectional view of the jet and the `circular wire' photograph of figure 3b make the entire shear layer visible. The small supports, which hold the wire in place, make non-uniform streamline spacing in all circular wire photographs. Both of these photographs show that the laminar shear layer, shed from the nozzle lip, rolls up into axisymmetric (m = 0), discrete vortices that grow in the streamwise direction. Each photograph covers a downstream distance of more than twice the jet diameter and within this distance laminar to turbulent transition of the shear layer through the growth of the instability waves and the large scale structures is clearly visible.

Swirling jet: Straight and circular smoke-wire photographs are presented in figure 4, which clearly shows that the swirling jet flow field is more complicated than that of a nonswirling jet. In order to facilitate discussion, straight wire visualizations, figures 4a and 4c are discussed first. The amount of swirl is visible from the turning angles of the streaklines in these photographs. However, the azimuthal motion in the counter-clockwise direction looking downstream turns the streaklines away from the reader in the left side of the jet and towards the reader in the right side of the jet. Due to this azimuthal motion, the streaklines along the outer edge of the jet, which carry information about the instability waves, move towards the center of the field of view and become difficult to isolate.

In figure 4a, for the Re = 20,000 jet, streaklines are initially smooth with very little diffusion; but in figure 4c (Re = 60,000 jet) they are completely mixed in the jet core starting from the nozzle exit. Later in the paper it is shown that the turbulence produced from the vortex bursting, which occurs inside the nozzle for the latter jet, causes this smearing of the streaklines.

The `circular wire' photographs of figures 4b and 4d show that the large-scale structures are present in the shear layer of the swirling jet, but are distorted by random three-dimensional structures. Compared to a nonswirling jet of similar Reynolds number, the streaklines lose their identity closer to the nozzle exit. Moreover, mode shapes of the large-scale structures are not clear in these photographs. The first two roll ups of figure 4b are predominantly axisymmetric and those of figure 4d are predominantly helical. In general, natural swirling jets contain relatively weak coherent structures, which are combinations of various mode shapes.

Another interesting difference between the swirling and the nonswirling jets under study is the shorter length of the quiescent state for the latter. This is the region between the nozzle exit and the first roll-up position where the amplitudes of the instability waves are relatively small. For the Re = 29,000 nonswirling jet (figure 3a and 3b), it is nearly two thirds of the jet diameter, while, for the swirling jet of lower Reynolds number (Re = 20,000, figure 4b), the first roll-up appears in half of that distance.

Vortex breakdown: Vortex breakdown appears in the jet core at all Reynolds numbers and is visualized through smoke insertion in the jet centerline (figure 5). The size, shape and the location of the breakdown zone change significantly with Reynolds number. At Re = 14,000, vortex bursting occurs nearly two diameters away from the nozzle exit. It moves upstream as the Reynolds number is increased, and eventually, at Re = 35,000, the bursting moves inside the tunnel. Visual observation indicates that the vortex breakdown location is always unsteady, but the associated frequencies are very low: below 2 Hz for the Re = 22,000 jet. The random unsteadiness produced by the vortex bursting is expected to be felt throughout the flow field. This, however, should not significantly affect the shear layer instability waves, which were predominantly in the frequency range of 15 to 60 Hz.

It is also observed that the vortex bursting location can be modified by placing a small probe at or near the vortex core upstream of the naturally observed bursting location. This causes the breakdown location to move upstream and to oscillate around the probe. However, the bursting location remains completely unaffected if the probe is kept approximately outside of r/D = 0.3. A detailed discussion of the probe interference effect can be found in Panda (1990). Due to this interference effect, no reliable measurement can be performed near the jet core upstream of the naturally occurring bursting location. Moreover, measurements in the vortex core downstream of the above location are also unreliable, since vortex bursting is always followed by a large recirculation zone (Faler and Leibovich 1978).

Vortex breakdown suddenly produces a large amount of turbulence at the jet core. As mentioned earlier, this makes a striking difference between the `straight wire' photographs of the swirling (figures 4a and

4c) and the nonswirling (figure 3a) jets. In contrast to the long smooth streaklines that persist through the potential core in a nonswirling jet, streaklines become completely mixed within one and a half diameters downstream from the vortex bursting location in a swirling jet. In the former, the shear layer at the outer edge of the jet grows radialy for 7 to 8 diameters downstream and finally merges at the centerline. In the latter, the extent of this potential core is much smaller. Upon interacting with the vortex breakdown flow field, the shear layer that grows along the outer periphery of the jet loses its coherence, and in general, "random turbulence" follows.

3.2 Mean flow measurements

Time-mean flow fields of the free swirling jets are surveyed at 8 axial locations between $0.12 \leq x/D \leq 2.5$ using a two-wire probe with the wires arranged in the form of a `V'. A particular problem with the V-wire probe is the large separation distance between the wires (about 2.2mm at the tip of the 'V' for the present probe). However, the orientation of the probe was such that the wires were normal to the radial direction. Therefore, the measured data are not affected by the velocity gradients in the radial direction.

A more important problem in the time-averaged measurement appeared due to the large flow angularity, which also changed continuously from the center to the outer edge of the swirling jet. To obtain reliable data using V-wire probe it was rotated about the axis. Typically, velocity surveys at every axial locations were performed two times. During the first survey the probe was kept at a fixed angle and approximate flow direction at various radial locations were determined. During the repeat survey, the probe was rotated to keep the mean flow direction within $\pm$ 15° of the V-angle bisecting direction. The contamination of the measured data by the radial velocity component is assumed to be small. This is supported by five-hole pitot probe measurements in swirling free jets by Farokhi *et al.* (1989), who showed that the radial velocity component is in general small except at the vortex core. The measurement from the vortex core is excluded from the data set presented in this paper due to significant probe-interference.

In addition to the above considerations the time averaged flow field is assumed axisymmetric. This is reasonable due to the circular geometry of the jet. Also, there is large number of swirl vanes placed too far upstream of the nozzle exit to introduce significant asymmetry. The large-scale instabilities, particularly the helical mode of the Kelvin-Helmholtz instability, have significant non-axisymmetry; however, the time mean flow field remains axisymmetric.

Figure 6 shows the time mean axial (U) velocity surveys for swirling jets of Reynolds number 22,000 and 57,000. Data are not presented in the region $0 \leq r/D \leq 0.13$, where the probe *significantly* contaminates the measurements. Presence of the swirl velocity component significantly modifies the U profiles. This is

especially true in the jet core, where there is either an extra axial momentum flux (jet-like behavior) or a deficiency of it (wake-like behavior) compared to the surrounding potential flow. For the lower Reynolds number case (Re = 22,000, figure 6a), the jet-like behavior is seen at the vortex core up to half a diameter downstream when it changes to a wake-like profile. However, the higher Reynolds number (Re = 57,000, figure 6b) jet shows wake-like axial velocity profiles at the jet centerline starting from the nozzle exit. In order to confirm this behavior of the U profiles, measurements are repeated with a single-sensor hot-wire probe oriented normal to the local flow direction. Again, velocity profiles similar to those of figure 6 are obtained. Such a change from jet- to wake-like axial velocity distribution in the vortex core was also observed before and after vortex breakdown by Faler and Leibovich (1978) and Chervinsky and Chigier (1966). The former measured the velocity distribution in a confined swirling jet using Laser Doppler Anemometry and the latter performed experiments in a free-swirling jet. An explanation for such behavior based on the combined effects of a rotating flow passing through an area contraction and vortex breakdown follows.

An inviscid analysis of the effect of a change of cross section of a tube on a stream of rotating fluid was performed by Batchelor (1967, section 7.5). According to this analysis, when certain fluid flows, having an initial, uniform axial velocity and rotating as a rigid body, passes through an area contraction, its axial velocity distribution becomes non-uniform. This is because the vortex lines, which are initially parallel to the axis, turn into a spirals during the passage through the area contraction. Thereby, an additional azimuthal component of vorticity is produced. This yields a negative value of $\partial U/\partial r$, so that a contraction of the stream tube produces a maximum of axial velocity at the axis. In the present swirl tunnel, the constant angle turning vanes give a rotation to the flow, which then passes through an area contraction. According to the aforementioned inviscid analysis, the exit flow should have a higher axial velocity at the tunnel center line (jet-like behavior). This is the case for the lower Reynolds number jet (Re = 22,000).

This scenario becomes more involved due to the presence of vortex bursting at the jet core. With the appearance of the vortex bursting, a free stagnation point appears in the jet centerline and a large reverse flow region follows. Hence, a momentum deficit (wake-like velocity profile) is observed after vortex bursting. For the Re = 22,000 swirling jet, vortex bursting appears nearly half a diameter downstream of the nozzle exit (figure 5b), which is also the location where the U distribution in the vortex core changes from jet-like to wake-like profiles. For the higher Reynolds number (57,000) swirling jet, vortex bursting occurs before the nozzle exit, inside the contraction section. Therefore, wake-like velocity profiles are seen at the jet center as close as the nozzle exit. These are seen in the mean axial velocity measurements of figure 6b.

The aforementioned discussion of the axial velocity distribution at the vortex core does not include the effect of the wake from the centerbody. The centerbody terminates less than two diameters upstream from

the nozzle exit. In a nonswirling jet, the wake from such a centerbody would produce a velocity defect at the center of the jet. To the contrary, figure 6a shows an increased axial velocity at the vortex core close to the nozzle exit for the Re = 22,000 swirling jet. It is believed that the momentum deficit of the wake from the centerbody is more than compensated for as the swirling flow passes through the contraction section. However, some trace of the wake may still remain in the region $0 \le r/D \le 0.13$, where measurements are unreliable and are not presented here.

The time mean azimuthal velocity profiles for Re = 57,000 swirling jet are shown in figure 7. Measurements at Re = 22,000 are almost identical and therefore not shown here. The azimuthal velocity component W behaves like a solid body rotation near the jet centerline. Away from the centerline the distribution is similar to a potential vortex. Numerical integration of the axial and tangential velocity profiles produces estimates of the swirl number, S, of 0.5 and 0.45 for Reynolds numbers of 22,000 and 57,000, respectively. In these cases the flow angle varies between 25° to 50° away from the shear layer. The higher value is found around two tenth of a diameter away from the jet centerline. The lower value is found just inside the lip shear layer. Smoke streaklines in the flow visualization photographs, presented earlier, also indicate similar mean flow angles.

Mass and momentum fluxes and momentum thickness: The mass flux ($M = 2\pi\int_0^\infty \rho U dr$), the axial momentum flux (G_x) and the tangential momentum flux (G_θ) for the swirling jet are calculated from the measured velocity profiles. The latter two quantities are defined in equation 2.3. Mass flux data are non-dimensionalized by their corresponding values at x/D = 0.12 (the measurement station closest to the nozzle exit) and are plotted in figure 8. Conservation of axial and angular momentum requires G_x and G_θ to remain constant at all axial stations. Since the measurements of the axial and the tangential velocity components around the jet centerline are unreliable, calculation of M, G_x and G_θ have some amount of uncertainty. In spite of this, it is observed that the measured axial and tangential momentum fluxes remain nearly constant at all axial stations (Panda 1990), which also brings credibility to the measured data.

For a swirling jet, if the radial velocity component is neglected, two components of the vorticity vector exist: the azimuthal component $\omega_\theta = -\partial U/\partial r$, and the axial component $\omega_x = \partial W/\partial r + W/r$. It is found, however, that in the shear layer of the swirling jets under study, the azimuthal component is considerably larger than the axial component. This can be seen clearly in the U and W distributions of figures 6 and 7. Close to the nozzle exit (x/D = 0.12), sharp U and W velocity gradients indicate the jet shear layer where the mean flow angle is about 11°. The velocity gradient associated with the W distribution is not only considerably smaller than that with the U distribution, but it also becomes unidentifiable earlier. Hence, in the

estimates of the vorticity thickness the contribution from the axial vorticity component ω_x is neglected.

For a given axial station, the vorticity thickness δ_ω is calculated from the axial velocity profile as $\delta_\omega = U/ du/dx_{max}$ and the momentum thickness θ is determined to be one-fourth of the vorticity thickness. The momentum thickness data, plotted in figure 9, are calculated at various axial stations for both the swirling and the nonswirling jets and non-dimensionalized by their values (θ_0) at x/D = 0.12. Since the outer shear layer in the Re = 57,000 swirling jet starts to interact with the vortex bursting flow field at about x/D = 0.75, θ is calculated only up to this axial station. The momentum thickness distribution of a non-swirling jet of Re = 60,000, produced from the same facility, is plotted in figure 9. This figure shows that θ increases approximately linearly for both the swirling and the nonswirling jets. However, it increases faster for the swirling jet, which once again indicates a faster spreading rate for this jet.

RMS velocity fluctuations: Figure 10 presents distributions of the root-mean-square axial (u_{rms}) and tangential (w_{rms}) components of the velocity fluctuations normalized by the mass averaged axial velocity U for the Re = 57,000 swirling jet. Close to the nozzle exit, higher levels of turbulence are found in the outer shear layer and in the vortex core, than in the annular region between them. Both axial and tangential velocity fluctuations at the nozzle exit are significantly high, which is believed to be due to the flow separation in the swirl vanes upstream from the nozzle. The maximum axial component of the turbulence fluctuations in the shear layer at x/D = 0.12 are 15% and 18% of the mass averaged axial velocity for Re = 22,000 and 57,000 swirling jets respectively. These values are comparable to the turbulence levels found in a fully developed, turbulent, free shear layer. However, the turbulent fluctuations associated with the tangential velocity component are somewhat lower; the initial levels are about 10% and 13% of the mass averaged axial velocity for Re = 22,000 and 57,000 swirling jets respectively.

The higher turbulence levels in the vortex core are clearly due to the unsteadiness produced by vortex bursting and the recirculation zone that follows. The regions of high turbulence from both the peripheral shear layer and the vortex bursting core spread radialy. Within a downstream distance of twice the jet diameter, a completely turbulent jet with both u_{rms} and w_{rms} levels as high as 22% of the mass averaged axial velocity emerges. The potential core is abolished and the spreading rate increases. This ability of a swirling jet to perform rapid mixing between the fluids in the vortex core and the jet periphery is absent in its nonswirling counterpart.

3.3 Velocity spectra of a natural swirling jet

Spectral evolutions of both swirling and nonswirling jets are measured in detail. A thorough

discussion of the latter can be found in Panda, 1990. The velocity spectra obtained in the natural swirling jet of Re = 22,000 are shown in figure 11. The Strouhal number St is based on the jet diameter and is defined as St = fD/U. Figure 11 shows six spectra of the fluctuating axial velocity component in the shear layer at various axial stations. Except for the axial station just downstream of the exit all spectra are similar and closely resemble those obtained from a fully developed turbulent shear layer. Unlike the nonswirling jet, they show neither a distinct peak nor any significant growth, which is characteristic of periodic, coherent motions. This implies that either the coherent structures are absent or they are too weak and random to leave a footprint in the velocity spectra. The flow visualization photographs presented in figure 4 support the latter conclusion, but they are not helpful in providing further information on the organized structures in a natural swirling jet. All of these facts clearly underline the difficulty in studying the organized structures in such a jet and the artificial excitation remains as the obvious practical way to study such structures.

3.4 Artificially excited jet

Acoustic excitation makes the organized structures regular and reduces phase jitter. Due to the high level of background random turbulence fluctuations, relatively high levels of acoustic excitation are used to achieve this goal. The sound pressure levels used for different Reynolds number jets appear in Table 1. In the following, the flow visualization photographs of swirling jets excited at different mode shapes will be presented first, followed by a detailed discussion of the quantitative measurements.

3.4.1 Flow visualization of excited swirling jet

Figure 12 shows a sketch of the co-ordinate axes, direction of the helical modes and the mean flow direction for the swirling jet. For the m = -1 mode the phase fronts follow a clockwise helix looking down-stream. This is opposite to the direction of mean flow swirl.

Figure 13 shows the multiple exposure, phase-locked photographs of the Re = 22,000 swirling jet excited with various mode shapes. A `circular smoke-wire' placed at the nozzle exit is used for all of the photographs. The excitation system successfully excites the axisymmetric and the helical (both m = +1 and -1) modes. Similar photographs taken for the Re = 57,000 swirling jet can be found in Panda (1990). Reasons for the choices of the particular Strouhal numbers are discussed later.

The excited swirling jet photographs are noticeably different from the unexcited jet photographs of figure 4. The organized structures have become prominent and the randomness is reduced. The higher excitation levels have forced the irregular, multimodal structures of the natural jet to become regular. The roll-ups are bigger; the first of them forms almost next to the nozzle exit. No indication of vortex pairing is

visible in these photographs, which cover a downstream distance of more than twice the jet diameter. Also note that the average inclination angle of the helical instability waves is about 13° with respect to a plane *normal* to the jet axis. This is comparable to the average swirl angle (~ 11°) measured in the shear layer around the jet.

3.4.2 Measurements in excited jets

A given Reynolds number jet is excited at various Strouhal numbers but at the same level of excitation in order to determine the range of frequencies in which the shear layer is receptive to the artificial excitation. Measurements are performed with axisymmetric (m = 0) and helical (m = -1 and +1) modes of excitation. The choices of the excitation frequency, level of excitation and the location of the probe to measure receptivity to upstream excitation, however, are involved. Since these variables are interdependent, several repetitions were necessary to reach the optimum values. Further discussion on the choice of excitation levels, excitation frequency and probe locations follows in that order.

For quantitative measurements, the amplitude of the excitation is chosen such that the organized structures are barely `tagged', so that the natural jet characteristics do not change significantly. As mentioned earlier, a relatively high level of acoustic excitation is needed to energize the large-scale structures sufficiently. Minimum excitation levels needed to produce a clear peak in the velocity spectra close to the nozzle exit (x/D = 0.12) of the Re = 22,000 and 57,000 swirling jets are 80 dB and 94 dB, respectively. Therefore, these excitation levels are used for all quantitative measurements. Flow visualization photographs, as well as hot-wire measurements of the mean velocity components in the shear layer, show no increase in the jet spread even at an excitation level of 92 dB for the Re = 22,000 jet. This supports an earlier observation of Taghavi and Rice (1989) that unlike a nonswirling jet, the spreading of a swirling jet cannot be easily affected by artificial excitation of the shear layer.

Figure 14 shows the result of excitation at various Strouhal numbers in the m = 0 mode on the Re = 57,000 swirling jet. Organization of the instability waves is indicated by the sharp spectral peaks at the excitation Strouhal numbers. For the same level of excitation, the strongest peak is observed when the jet is excited at St = 1.5 (56 Hz). The peaks become weaker for both higher and lower excitation Strouhal numbers. Excitation above St = 2.5 has no effect on the velocity spectra of the Re = 57,000 jet. A summary of the final results for swirling jets of two different Reynolds number is given in Table 2.

The lowest excitable Strouhal number is limited by the excitation system, which includes four 25.4 cm diameter woofers that are essentially ineffective below 14.5 Hz. This is a serious problem for the 22,000 Reynolds number jet, where the spectral peak becomes stronger as the excitation Strouhal number is reduced.

It is the strongest at the lowest excitable Strouhal number of 1.0 (14.5 Hz). Again, for the Re = 22,000 jet, excitation above St = 2.5 does not produce a peak in the velocity spectra, indicating that the shear layer is not receptive to excitation above this Strouhal number.

Tam and Morris (1985) developed a quasi-linear model to predict the receptivity of the instability waves in a nonswirling jet to upstream excitation. Their theoretical predictions show very favorable agreement with the experimental results (Lepicovsky *et al.* 1985) over a wide range of excitation frequencies and excitation levels. According to their model, the highest receptivity occurs when the excitation frequency is close to the frequency of the most unstable wave in the natural shear layer. The amplitudes of the large-scale structures decrease as the excitation frequency moves away from this most receptive frequency (keeping the excitation level constant). By extending this observation for the present swirling jets, it appears that the most unstable waves close to the nozzle exit are around St = 1.0 and 1.5 for the Re = 22,000 and 57,000 jets, respectively.

Most of the measurements to determine the characteristics of the instability waves are performed at the above mentioned two Strouhal numbers where the swirling jets are most receptive to the acoustic excitation. Figure 15 shows the variation of the axial velocity spectra along the downstream direction for the Re = 22,000 swirling jet excited at St =1.0. Except for the slow growth and subsequent decay of the excited instability waves, the velocity spectra are nearly identical at all axial stations. The highest amplitude of the St = 1.0 wave in the Re = 22,000 jet is reached around x/D = 0.5 and that of the St = 1.5 in the Re = 57,000 jet is reached around x/D = 0.35. Therefore, these two axial locations are chosen to determine the receptivity of the respective swirling jets to various excitation frequencies. Experiments are also conducted to determine the most receptive frequencies of the helical modes. Results similar to those of Table 2 were also obtained for such modes.

3.4.4 Evolution of instability waves

The evolution of instability waves is measured at the half velocity points of the peripheral shear layer and at various streamwise locations using two different techniques: the phase averaging technique and the band-passed spectral technique.

The phase reference for the first technique is obtained from one of the speaker input signals. More than 100 cycles are used to calculate the phase averaged velocity components. The phase averaging process provides information not only about the phase locked excited wave but all of its harmonics as well. "Contamination" can be a problem if the amplitudes of the harmonics are comparable to that of the excited wave. Thus, the phase averaged velocities are Fourier transformed to separate contributions from the fundamental and

various harmonics of the excitation frequency. Details of the data processing are discussed in the thesis of Panda (1990). The Fourier transform also produces the phase relation between a particular wave and the reference signal used for the phase averaging process. All phase averaged data presented in this paper are Fourier transformed and the variables representing such data are expressed within angle brackets (e.g. $<u_{rms}>$).

In the band passed spectral technique, the growth of a given frequency band is calculated from the power spectral density (PSD) of the velocity fluctuations similar to those shown in figures 14 and 15. Usually, a 2.5 Hz wide band centered around the desired frequency, whose evolution is to be calculated, is chosen and the energy contained in this band is determined from the velocity spectra. The square root of this energy produces an estimate of the turbulent fluctuations associated with the waves in the particular frequency band and is referred to as the band passed turbulent fluctuation. In this text, variables representing such data are expressed in parentheses, e.g., (u_{rms}).

The rms values of the phase-averaged axial component of velocity for the Re = 22,000 jet excited at St = 1.0 and at various mode shapes are presented in figure 16. A considerably higher growth rate of the helical modes over the axisymmetric mode is visible in this figure. The maximum amplitude of both the axisymmetric and the helical modes occurs around x/D = 0.5. At this location, the coherent fluctuations are about 40% of the total turbulent fluctuations when the jet is excited in the helical mode, and 25% when the excitation is in the axisymmetric mode. In spite of the substantial coherence, overall growth of the instability waves from the initial level at x/D = 0.12 to the final saturation level at x/D = 0.5 is only within a factor of five which is much lower than that seen in a nonswirling jet.

Figure 17 shows the rms value of the phase averaged axial component of the turbulence fluctuations in the Re = 57,000 swirling jet. All modes are excited at St = 1.5 (56 Hz.). Again, all modes have a substantially high initial coherence but moderate overall growth; however, unlike the Re = 22,000 swirling jet, overall growth of the axisymmetric mode is nearly equal to that of the helical modes. Maximum coherence of about 25% of the total turbulent fluctuation occurs relatively closer to the nozzle exit, at x/D = 0.35.

According to Squire's theorem for an incompressible, parallel shear flow, the 2-D Kelvin-Helmholtz waves, whose wave fronts are normal to the flow direction, should have a higher amplification rate than oblique or 3-D waves of the same wave number. The amplification rates of 3-D waves fall slowly as the inclination angle with the normal direction increases (Drazin and Reid 1981). Intuitively, this idea of the most unstable mode being the one which produces roll-ups normal to the mean flow velocity vector can be extended to a swirling jet. Figure 12 shows that the m = -1 mode is normal to the swirl flow direction. Therefore, it should have the highest amplification rate and m = +1 should have the lowest. The phase averaged measurements shown in figures 16 and 17 do not support this argument. Measurements show that

both m = +1 and -1 modes have nearly equal growth rates. Flow visualization photographs of excited swirling jets also confirm this result. A possible explanation for this unexpected behavior is as follows.

The swirling jet under study has a very low degree of swirl in the shear layer around the periphery; the average flow direction in the shear layer is about 11° with the axial direction. Thus, the shear associated with the axial velocity component is much stronger than that with the tangential velocity component. Moreover, a relatively high level of acoustic excitation was used for the present experiment. Therefore, it is believed that the shear layer of the swirling jet under study behaves similar to that of a nonswirling jet where the axisymmetric and the helical modes have nearly the same amplification rates (Michalke 1984, Morris 1976).

Figure 18 shows the evolution of the subharmonic (St = 0.5, 7.5 Hz.) instability waves when the Re = 22,000 swirling jet is excited at St = 1.0, for various modes. The band passed turbulence fluctuations is determined from the axial velocity spectra at various axial stations (including the ones shown in figure 15). Surprisingly, the subharmonic waves of all modes show very little growth. This result is very different from that seen in a nonswirling jet, where the first subharmonic grows more than the fundamental instability wave (Michalke 1984, Panda 1990). The small growth of the subharmonic wave in a swirling jet also implies a suppression of vortex pairing. This is somewhat supported by the flow visualization photographs (figure 13) where indications of vortex pairing, such as an increase of the wavelengths of the organized structure at farther downstream locations, are not visible. Taghavi and Rice (1989) also made similar observations in their limited experiments in a higher Reynolds number swirling jet.

An important reason behind the small overall growth of the instability waves and the suppression of the vortex pairing in a swirling free jet is *a faster growth of the momentum thickness*. In this case, a disturbance, which is unstable at a given axial station, becomes neutrally stable within a short downstream distance. Therefore, the factor by which an instability wave grows in a swirling jet shear layer is much lower than that seen in a nonswirling jet, which has a much slower momentum thickness growth. Mankbadi (1985) showed that the fundamental-subharmonic interaction mechanism, leading to the nonlinear amplification of the subharmonic is significant only at low momentum thickness. The rapid growth of the momentum thickness in a free-swirling jet diminishes the fundamental-subharmonic interaction mechanism and is a reason behind the very small growth of subharmonics.

All of figures 16, 17 and 18 show that the phase averaged turbulent fluctuations, indicating coherent motion, become negligible within one diameter downstream from the nozzle exit. This is also the approximate location where the random turbulence from vortex bursting at the jet core starts to influence the shear layer development. Vortex bursting appears to help the decay of the organized motions and `random turbulence'

follows.

In a nonswirling jet, vortex pairing and entrainment due to the large-scale structures are the principal mechanisms by which the jet spreads and the momentum thickness grows (Browand and Laufer, 1975). As mentioned earlier, instability waves do not grow as much in a swirling jet, and vortex pairing is suppressed. Therefore, the large entrainment and spread rates of a free swirling jet cannot be explained from the dynamics of the organized structures alone.

One possible answer may lie in the relaxation of the radial pressure gradient (Farokhi *et al.* 1989). As the jet develops, viscous dissipation reduces the maximum swirl velocity inside the jet. This causes a relaxation of the radial pressure gradient and the jet spreads outwardly. According to this explanation, a swirling jet should spread without much entrainment of the ambient fluid. Yet, figure 8 shows that the entrainment is also higher in a swirling jet. Therefore, the relaxation of the pressure gradient also fails to provide a satisfactory explanation of the high entrainment rate of a swirling jet.

Another possible explanation may lie in the presence of centrifugal instabilities in the shear layer around the jet. Taylor-Gortler type instabilities in the form of longitudinal "braids" along the flow direction were observed experimentally in a curved, two-dimensional shear layer where the axial velocity decreases away from the center of curvature (Wang 1984, Ramjee *et al.* 1988). Such instabilities inhibit the growth of Kelvin-Helmholtz type instability waves but cause higher entrainment of fluid from the undisturbed flow. The shear layer formed at the outer periphery of a free-swirling jet is similar to a two-dimensional curved shear layer where both axial and tangential velocity components decrease radialy outward, away from the center of curvature. Therefore, centrifugal instabilities may be naturally present in a free-swirling flow. However, a detailed study of this instability is beyond the scope of the present work and is not explored further.

Wavelength and phase speed measurements: These two quantities, tabulated in Table 3, are estimated from the flow visualization photographs for the Re = 22,000 jet and are measured from the phase averaged data for the Re = 57,000 case. First, the wavelength λ is calculated and then the phase speed C_{ph} is determined from the known excitation frequency. The axial phase angle variation of the instability waves of various Strouhal numbers, shown in figure 19, is calculated from the phase-averaged data, discrete Fourier transformation of which produces a phase relation between the reference signal and the particular instability wave under study. The phase-averaged data are collected at various downstream locations keeping the radial position of the probe fixed (r/D = 0.494). The wavelength of the instability wave under consideration is the axial distance in which the phase angle changes by 360°. For most of the cases, the measured phase speed is about 60% of the

mass averaged axial velocity, which is also the phase speed of the most unstable wave in a nonswirling jet (Michalke 1984).

4. Conclusions

Large scale organized structures similar to those present in a nonswirling jet are studied in a swirling free jet in the Reynolds number range of 20,000 to 60,000. The integrated swirl number S is relatively high and is kept nearly constant between 0.45 and 0.5. The major observations and inferences obtained from this study are as follows:

1. Flow visualization photographs of the natural swirling jets show weak and very irregular large-scale structures in the shear layer around the jet. However, acoustic excitation is successfully used to produce regular organized structures in both helical (both m = +1 and -1) and axisymmetric modes. Phase locked multiple exposure photographs confirm the existence of such structures. Close to the nozzle exit most receptive instability waves are at St = fd/U = 1.0 and 1.5 for the Re = 22,000 and 57,000 swirling jets, respectively.

2. Phase averaged measurements in the excited swirling jets show that the overall growth of instability waves of all modes is small and subharmonic formation through vortex pairing is suppressed. An important reason for such behaviors of a swirling jet is a rapid growth of momentum thickness, which reduces growth of an unstable disturbance (Michalke, 1984) and suppresses the fundamental-subharmonic interaction mechanism (Mankbadi, 1985). Phase averaged measurements also show that both m = -1 and +1 helical modes have nearly equal overall growths in spite of a preferred direction of rotation imposed by the swirling motion.

3. Vortex bursting plays a very important role in a swirling jet and makes the development of such a jet completely different from its nonswirling counterpart. Time mean measurements and flow visualization photographs show that vortex bursting produces high turbulence fluctuations that spread rapidly outward from the vortex core to the shear layer around the jet. A faster decay of the coherent structures takes place when this random turbulence field interacts with the shear layer. For the present swirling jet, the potential core is lost and a completely turbulent jet emerges within two diameters downstream from the nozzle exit. The spreading and the mass entrainment rates as well as the growth rate of the shear layer momentum thickness are higher for a swirling jet than a nonswirling one.

The flow field of a swirling jet is far more complex than that of a nonswirling jet and many aspects of the shear-layer development, such as the completely featureless velocity spectra of the natural jet, the difficulty in exciting any natural modes and the large mixing and mass entrainment rates in spite of a small

growth of the organized structures, cannot be explained by the traditional Kelvin-Helmholtz type instabilities alone. It is believed that the centrifugal instabilities, that arise due to the curvature of the shear layer caused by the mean swirl, may be naturally present and have played an important role in the development of the free swirling jets. However, a thorough study of the centrifugal instability is needed to qualify the above conjecture. This also points out the direction for future research on this flow field.

Acknowledgements

The authors wish to acknowledge the support received from the National Science Foundation, through Grant No. ISI-8560806, and the donation of the developed facility by Dynamics Technology, Inc. The first author also acknowledges the support of the National Research Council, USA, for an NRC associateship held during the preparation of the manuscript.

REFERENCES

Batchelor, G.K. 1967 An introduction to fluid dynamics, *Cambridge University press.*

Bechert, D. and Pfizenmaier, E. 1976 On the amplification of broadband jet noise by a pure tone excitation. *AIAA paper no. 76-489*.

Browand, F.K., and Laufer, J. 1975 The role of large scale structures in the initial development of circular jets. *In Proc. 4th Symposium on Turbulence in liquids, Univ. of Missouri-Rolla*. 333-344.

Chervinsky, A. and Chigier, N.A. 1966 On similarity of axisymmetric swirling jets. TAE report no. 52, Technion - Israel Institute of Technology.

Cimbala, J.M. 1984 *Ph.D. thesis, California Institute of Technology*.

Corke, T., Koga, D., Nagib, H. 1977 A new technique for introducing controlled sheets of streaklines in wind tunnels. *IEEE publication 77-CH1251-8AES.*

Drazin, P.G. and Reid, W.H. 1981 Hydrodynamic instability. *Cambridge University Press*.

Faler, J.H. and Leibovich, S. 1978 An experimental map of the internal structure of a vortex breakdown. *J. Fluid Mech.* **86**, part 2, 313-335.

Farokhi, S., Taghavi, R., Rice, E.J. 1989 Effect of initial swirl distribution on the evolution of a turbulent jet. *AIAA J.* **27**, No. 6, 700-706.

Gupta, A. K. and Lilley, D.G. 1985 Flow field modelling and diagnostics. *Abacus press*.

Hussain, A.K.M.F. and Zaman, K.B.M.Q. 1985 An experimental study of the organized motions in the turbulent plane mixing layer. *J. Fluid Mech*. **159**, 85 -104.

Khorrami, M.R. 1991 On the viscous modes of instability of a trailing line vortex. *J. Fluid Mech.* **225**, 197-212.

Kibens, V. 1979 Discrete noise spectrum generated by an acoustically excited jet. *AIAA J.* **18**, No. 4, 434-441.

Leibovich, S. and Stewartson, K. 1983 A sufficient condition for the instability of columnar vortices. *J. Fluid Mech.* **126**, 335-356.

Lessen, M., Singh, P.J. and Paillet, F. 1974 The stability of a trailing line vortex, Part 1. *J. Fluid Mech*. **63**, 753-763.

Lepicovsky, J., Ahuja, K.K. and Burrin, R.H. 1985 Tone excited jets, Part III: Flow Measurements. *J. Sound and Vibration*.

Mankbadi, R.R. 1985 On the interaction between fundamental and subharmonic instability waves in a turbulent round jet. *J. Fluid Mech.* **160**, 385-419.

Michalke, A. 1984 Survey on jet instability theory. *Prog. Aerospace Sci.* **21**, 159-199.

Morris, P.J. 1976 The spatial viscous stability analysis of axisymmetric jets. *J. Fluid Mech*. **77**, 511-529.

Panda. J. 1990 Experiments on the instabilities of swirling and non-swirling free jets. *Ph. D. thesis*, The Pennsylvania State Univ.

Ramjee, V., Tulapurkara, E.G. and Rajasekar, R. 1988 Development of airfoil wake in a longitudinally curved stream. *AIAA J.* **26**, no. 8. 948-953.

Rhode, D.L. 1981 Predictions and measurements of isothermal flow fields in axisymmetric combustor geometries. *Ph. D. thesis*, *Oklahoma State University*.

Rose, W.G. 1962 A swirling round turbulent jet, 1 - mean velocity measurements. *J. Applied Mech, Transaction of ASME*. 615-625.

Sislian, J.P. and Cusworth, R.A. 1986 Measurements of mean velocity and turbulent intensities in a free isothermal swirling jet. *AIAA J.* **24**, no. 2, 303-331.

Taghavi, R. and Rice, E.J. 1989 Large amplitude acoustic excitation of swirling turbulent jets. *AIAA paper no. 89-0970.*

Tam, C.K.W. and Morris, P.J. 1985 Tone excited jets, Part V : A theoretical model and comparison with experiment. *J. Sound and Vibration*. **102(1)**, 119-151.

Wang, C. 1984 The effect of curvature on turbulent mixing layers. *Ph.D. Thesis, California Institute of Technology*.

Westphal, R.V. and Mehta, R.D. 1984 Crossed hot-wire data acquisition and reduction system. *NASA TM 85871*.

Table 1. Operating conditions of swirling jet experiments with excitation

Re	S		A	dB level
22,000	0.5	Flow Vis.	0.04%	86
		Measurements	0.02%	80
57,000	0.45	Flow Vis.	0.07%	98
		Measurements	0.04%	94

Table 2. Summary of results of swirling jet excitation

		Re=22,000	Re=57,000
Excit. amplitude (Measurements)		80 dB A=0.02%	94 dB A=0.04%
Most receptive	St =	1.0	1.5
	f =	14.5 Hz.	56 Hz.
Axial location x/D =		0.5	0.35

Table 3. Wave properties for swirling jet

Re	St.	Source	λ/D	C_{ph}/U
22,000	1.0 (m = 0)	Fig. 13b (Flow Viz.)	0.67	0.67
	1.2 (m = -1)	Fig. 13a (Flow Viz.)	0.61	0.73
57,000	1.5 (m = -1)	Fig. 19 (Phase meas.)	0.38	0.57
	1.0 (m = -1)	Fig. 19 (Phase meas.)	0.58	0.58
	0.75 (m = -1)	Fig. 19 (Phase meas.)	0.83	0.62

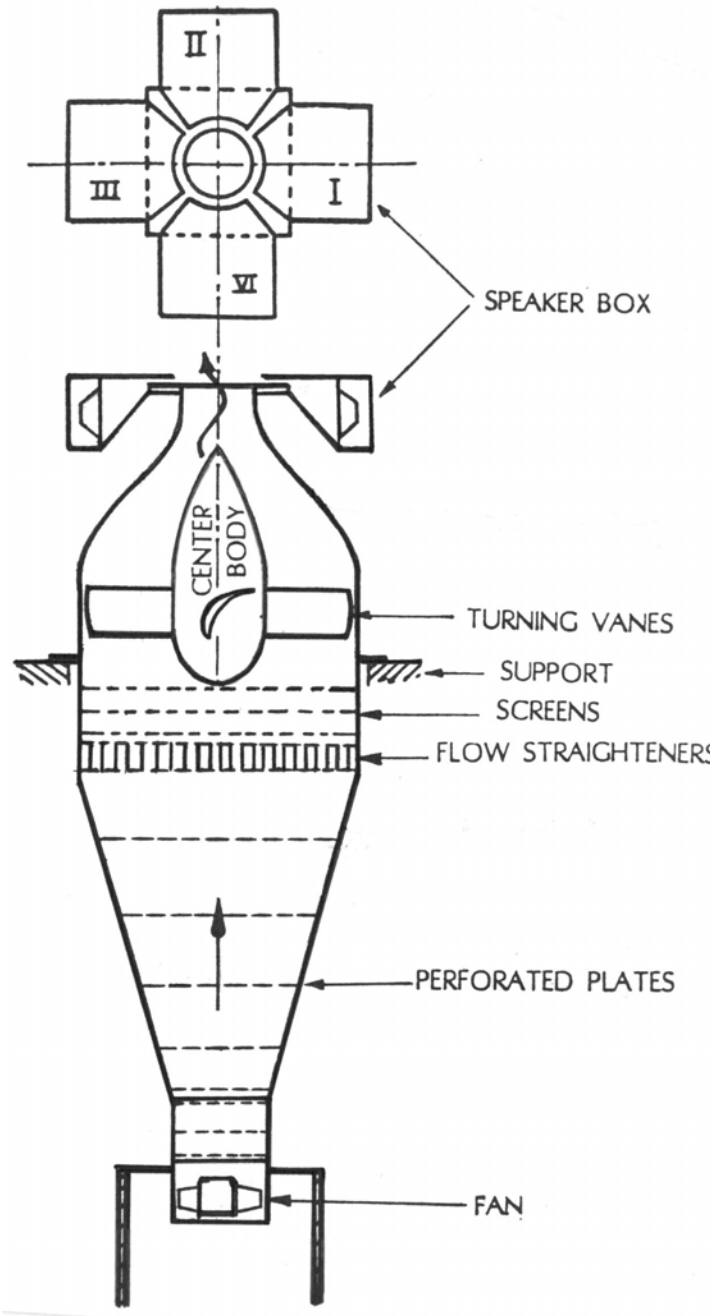

Figure 1. Schematic of the free jet facility.

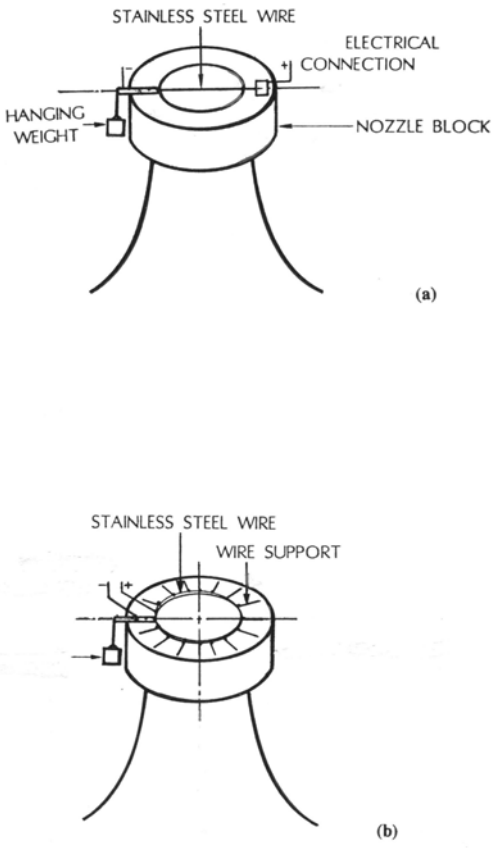

Figure 2. Smoke-wire flow visualization set-up. (a) Straight wire; (b) Circular wire.

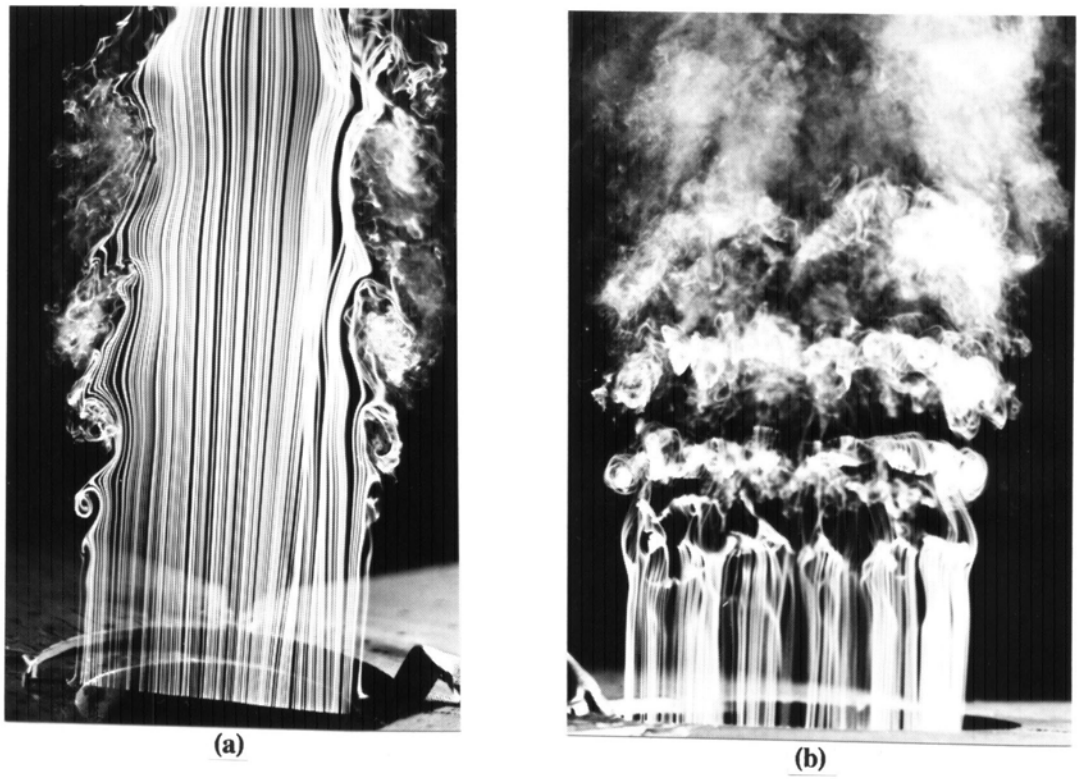

Figure 3. Smoke-wire photographs of Re = 29,000 natural *non-swirling jet.* (a) straight wire; (b) circular wire.

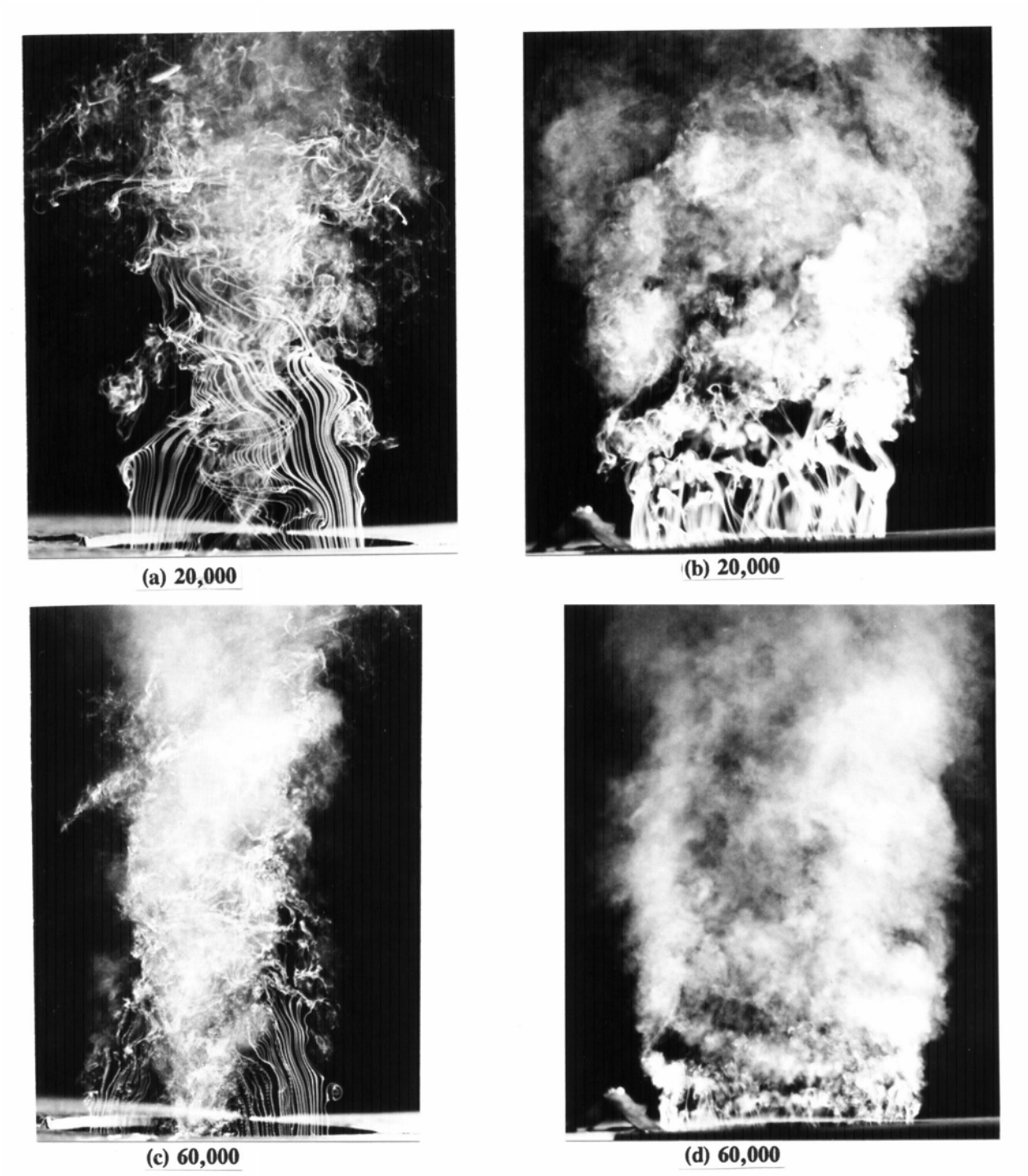

Figure 4. Natural *swirling jet* photographs at indicated Reynolds numbers. (a) & (c) Straight wire; (b) & (d) Circular wire.

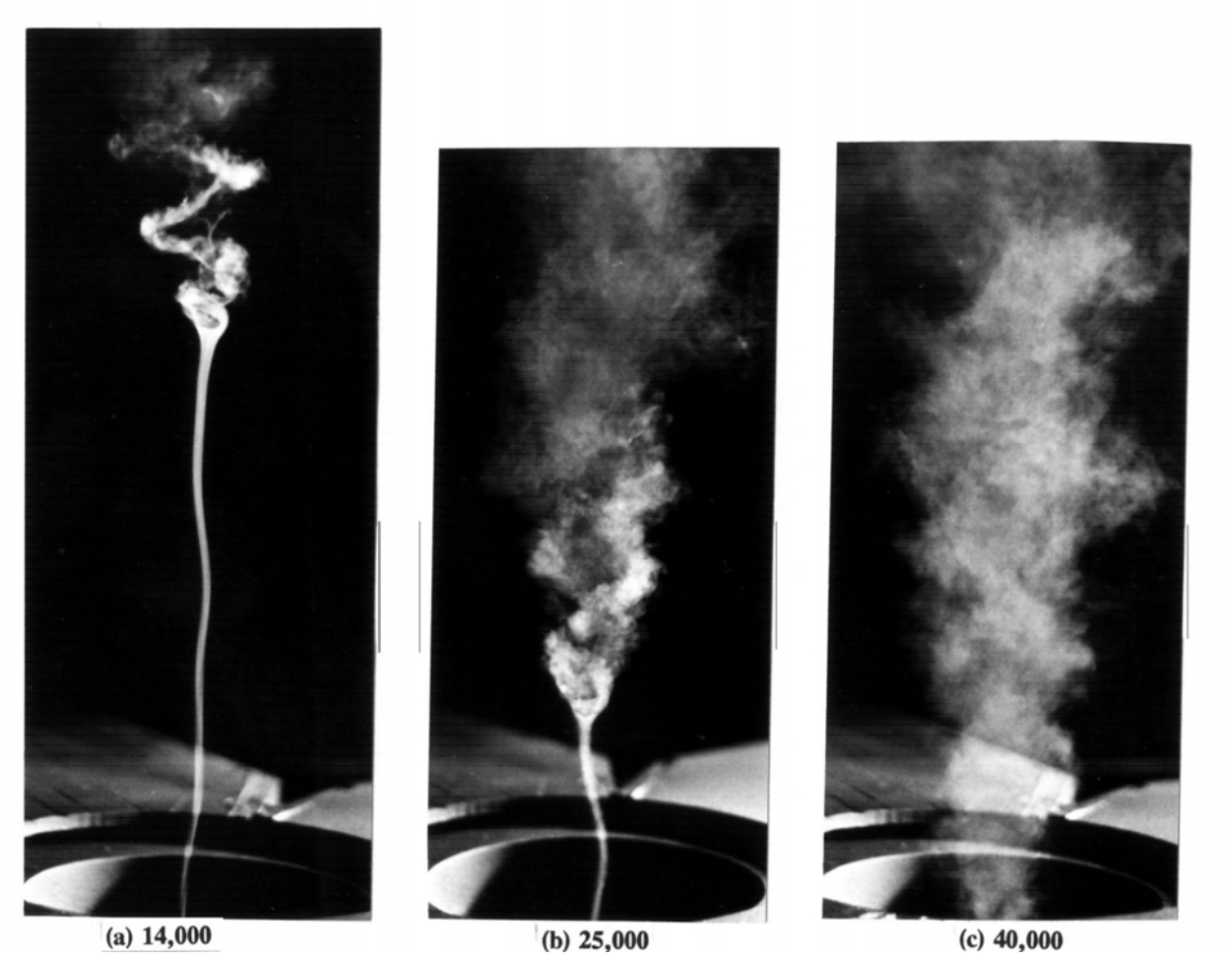

Figure 5. Vortex bursting at indicated Reynolds numbers. Smoke injected at vortex core only.

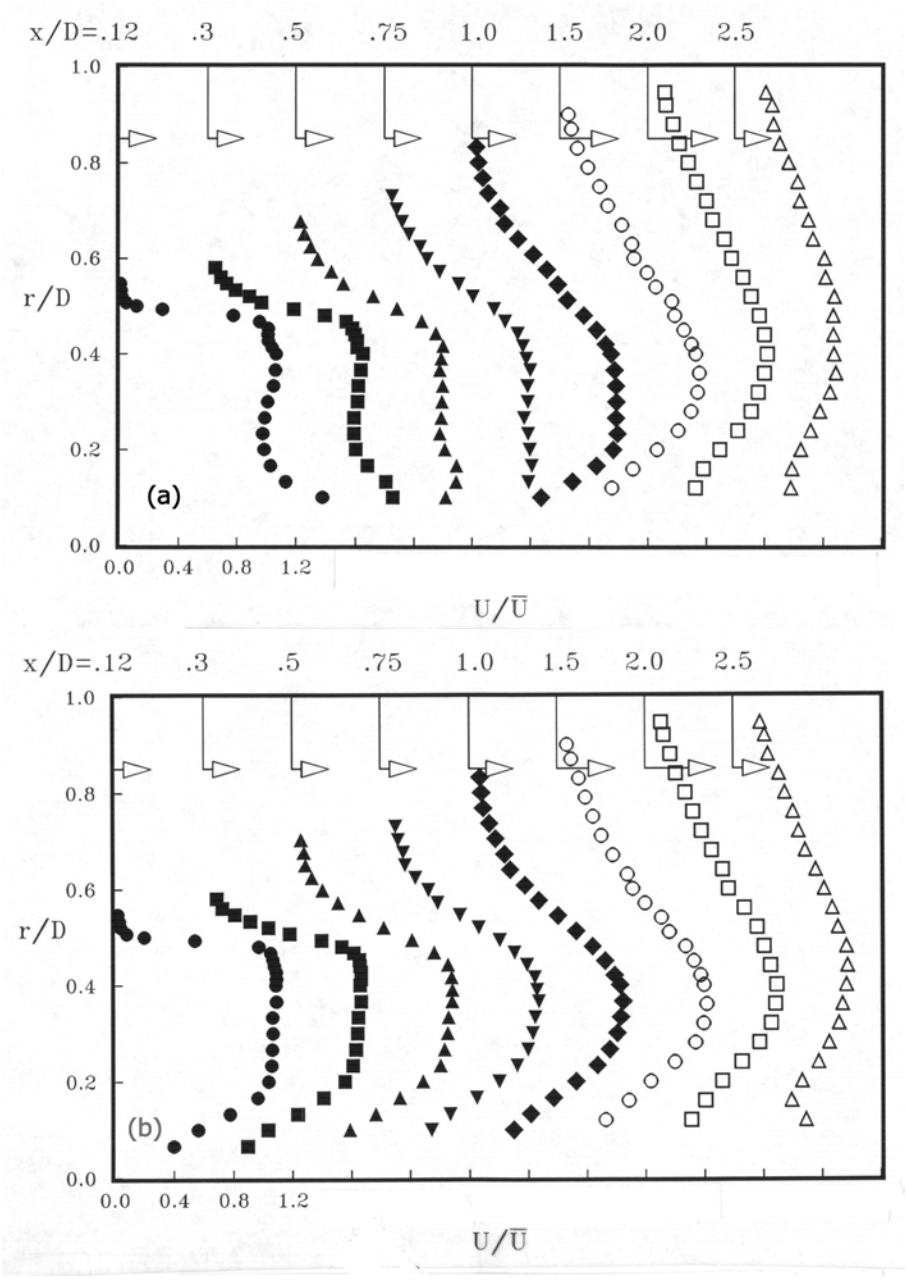

Figure 6. Time averaged axial velocity survey. (a) Re=22,000, S *=0.5;* (b) Re=57,000, S *=0.45.*

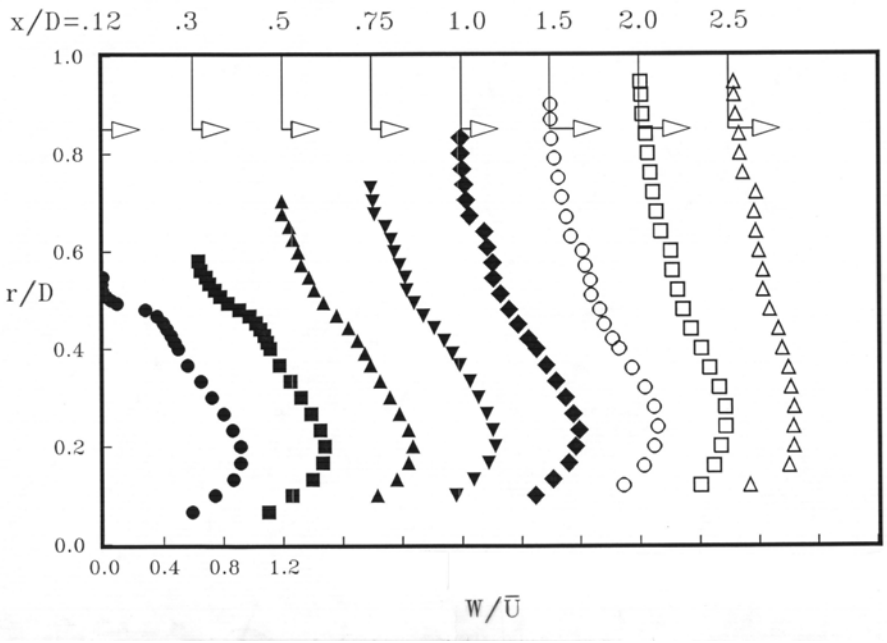

Figure 7. Time averaged tangential velocity survey. Re=57,000, S *=0.45.*

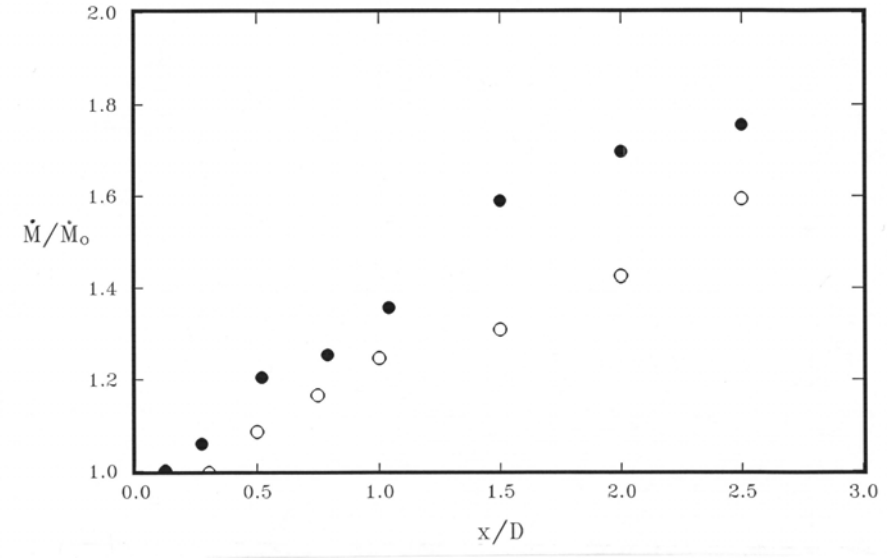

Figure 8. Mass flux calculated from the axial velocity surveys.o, non-swirling jet, Re=60,000; •, swirling jet, Re=57,000.

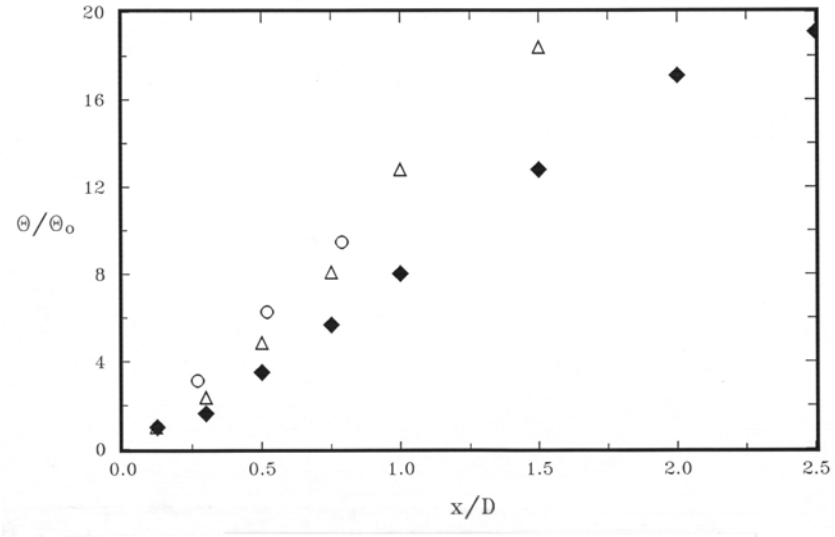

Figure 9. Momentum thickness variation with the downstream distance. ♦, non-swirling jet, Re=60,000; Δ, swirling jet, Re=22,000; O, swirling jet, Re=57,000.

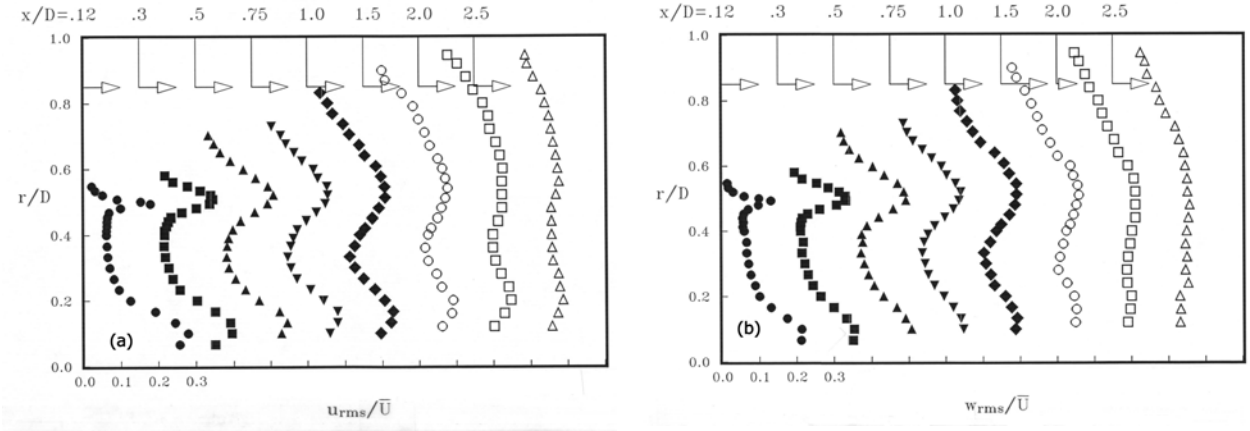

Figure 10. Time-mean velocity fluctuations; Re=57,000, S =*0.45.* (a) axial component; (b) tangential component.

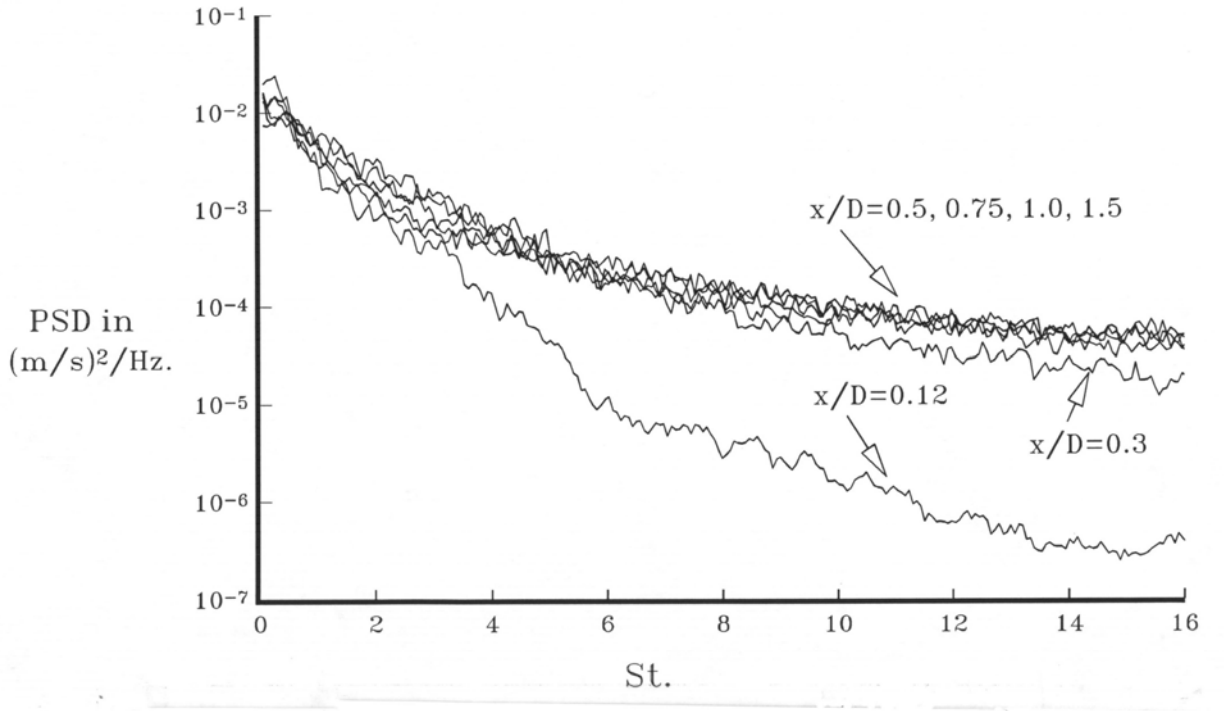

Figure 11. Velocity spectra in the shear layer of a natural swirling jet (Re =22,000) at indicated axial stations.

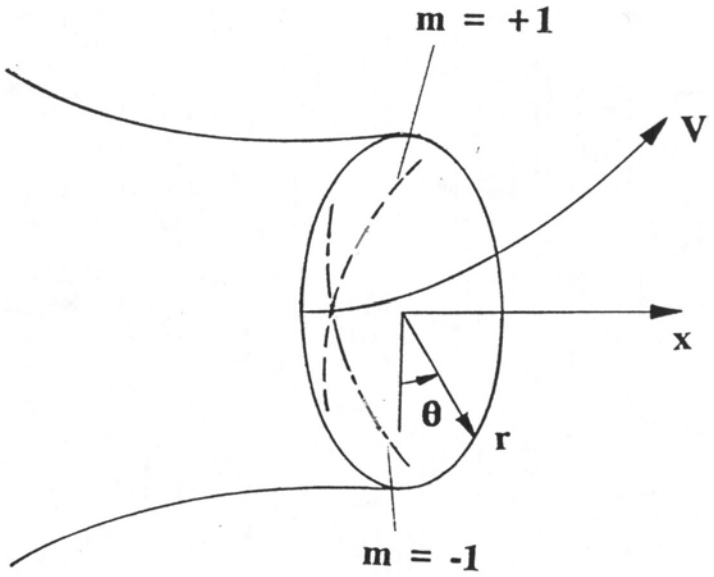

Figure 12. Sketch of the co-ordinate axes and various helical modes.

Figure 13. Phase locked multiple (17) exposure photographs of Re = 22,000 swirling jet excited at 86 dB; modes and Strouhal numbers of excitation are indicated.

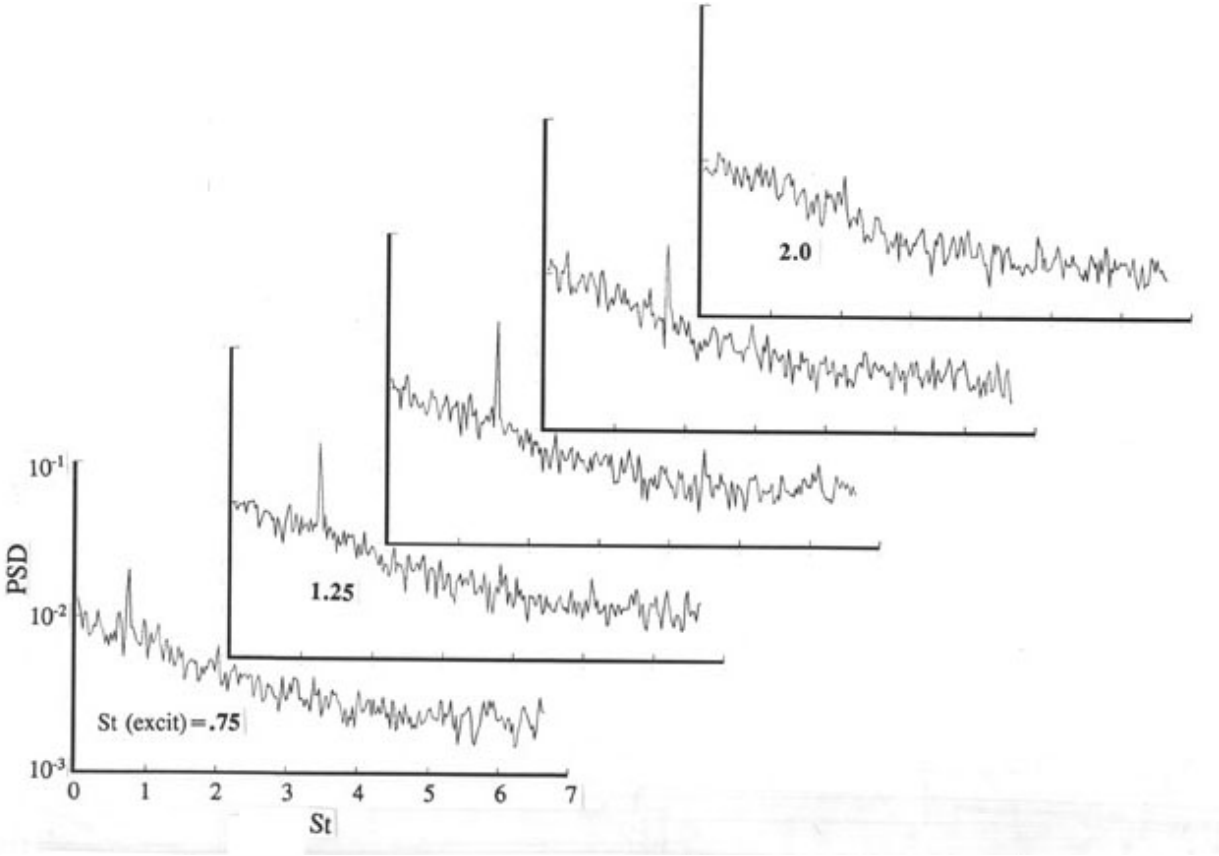

Figure 14. Velocity spectra obtained from Re=57,000 swirling jet at x/D=0.3 and r/D =0.51 for indicated excitation Strouhal numbers. Fixed excitation level of 94 dB in m =0 mode is used for all cases.

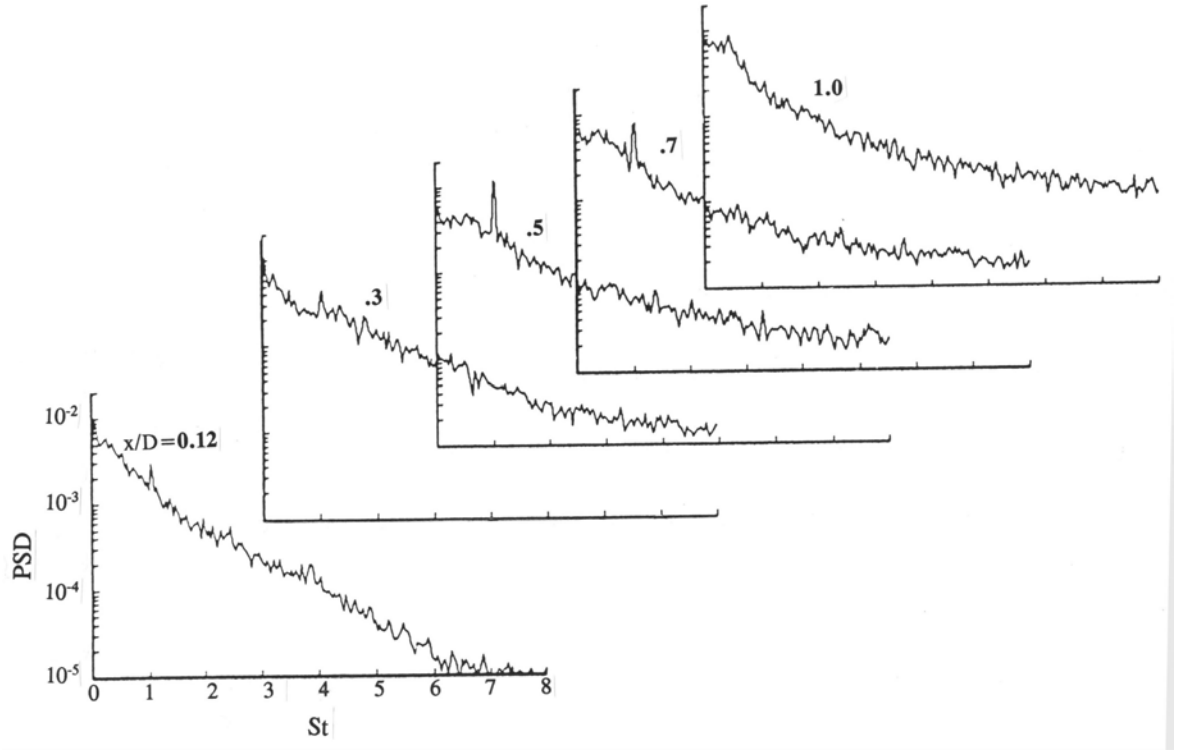

Figure *15.* Velocity spectra at *r/D =0.5* and at indicated axial stations when Re=22,000 swirling jet is excited at St=1.0 in m=0 mode; level: 80 dB.

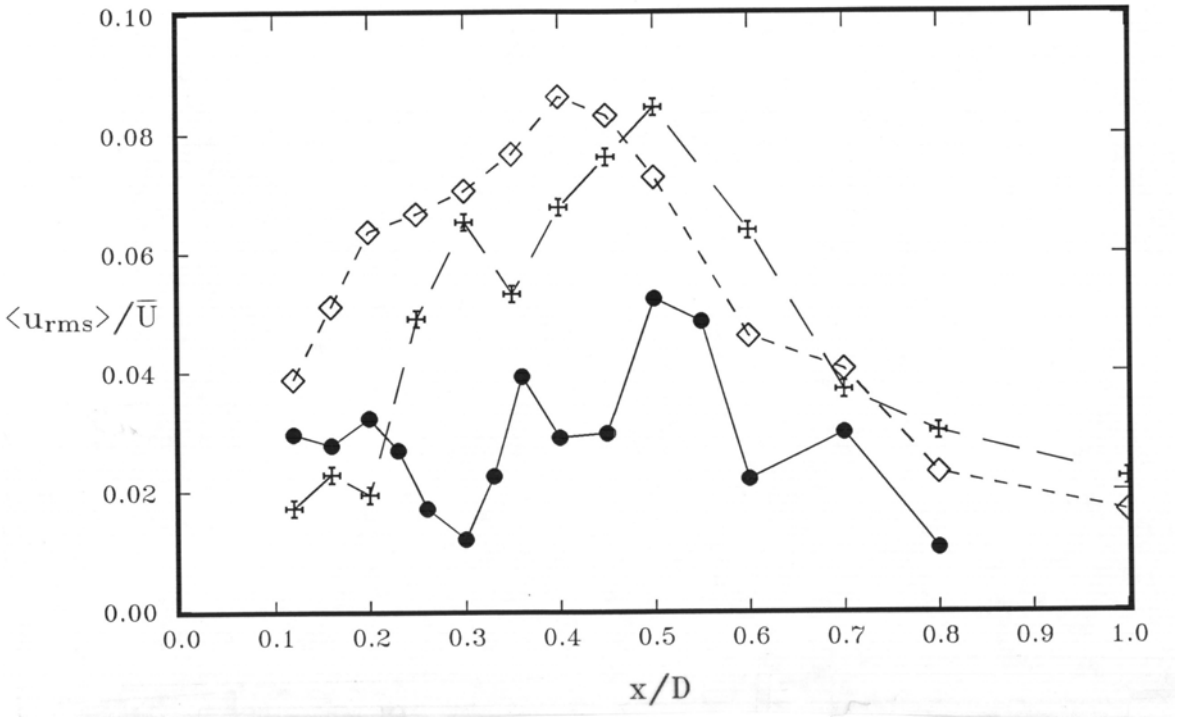

Figure 16. Evolution of the St. = 1.0 instability wave obtained through phase averaged measurement in Re = 22,000 swirling jet. + +, m = -1 mode; • • m = 0 mode; ◊ ◊ m = +1 mode.

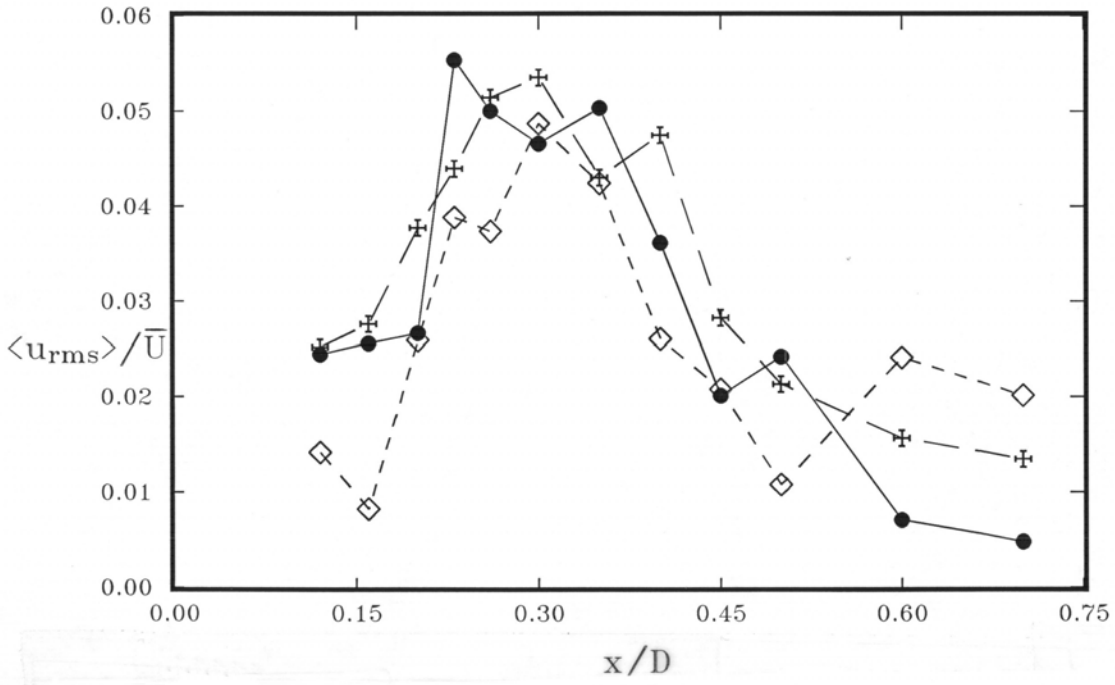

Figure 17. Evolution of the phase averaged axial velocity fluctuation of the St. = 1.5 (56 Hz.) instability waves in Re = 57,000 swirling jet. + + , m = -1 mode; ● ● , m = 0 mode; ◊ ◊ , m = +1 mode.

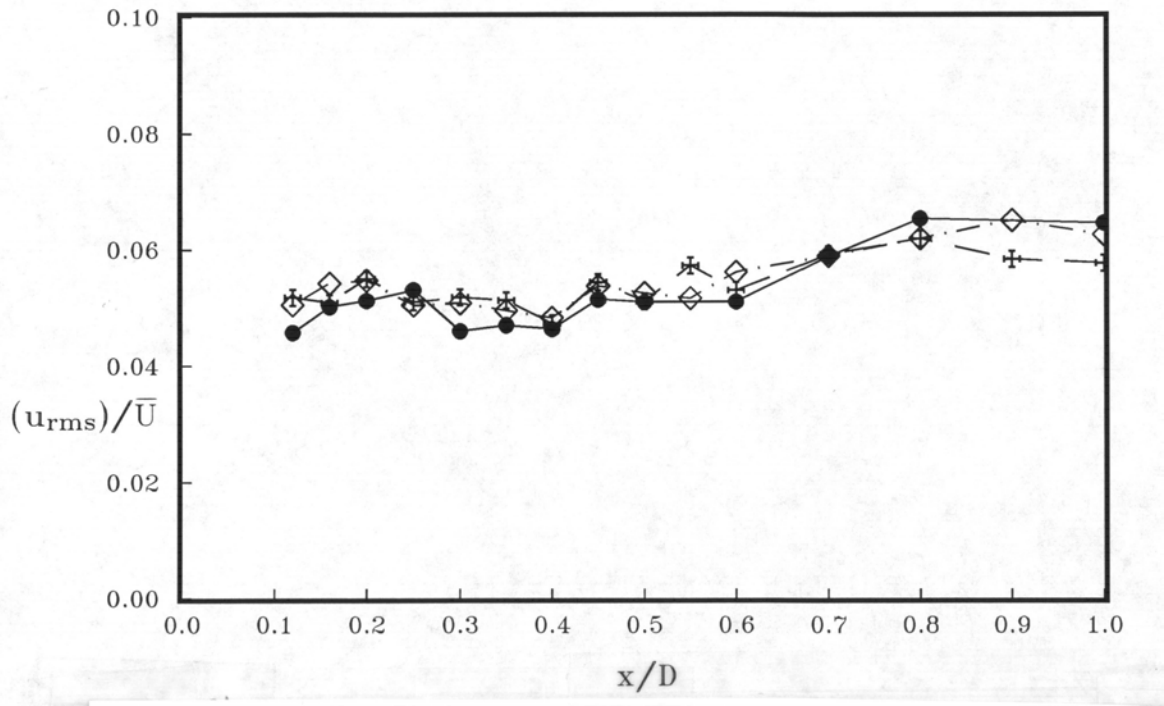

Figure 18. Evolutions of the subharmonic St. = 0.5 instability waves when Re = 22,000 swirling jet is excited at St = 1.0. + + , m = -1 mode; ● ● , m = 0 mode; ◊ ◊ , m = +1 mode.

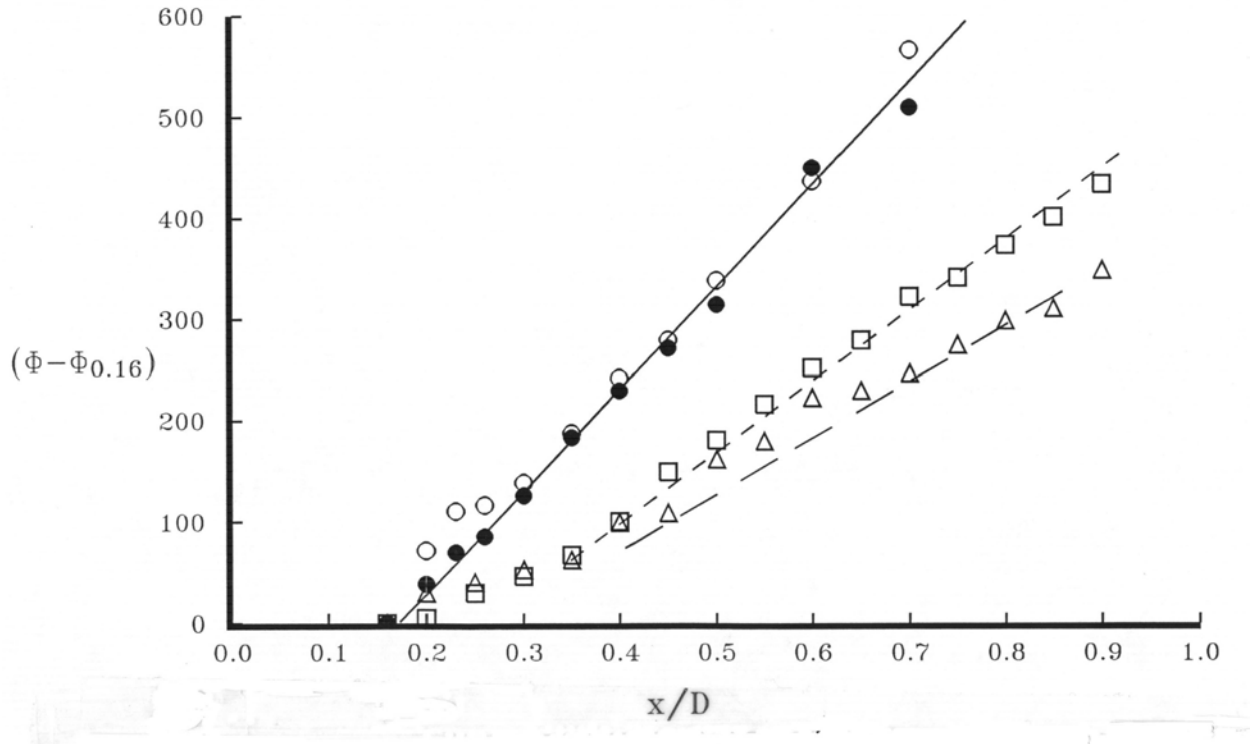

Figure 19. Phase variation of the helical (m = -1) mode waves along the axial direction in Re = 57,000 swirling jet. ○ ●, St = 1.5; □, St = 1.0; Δ, St = 0.75.